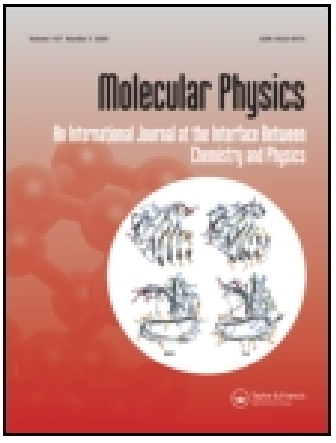

Molecular Physics: An International Journal at the Interface Between Chemistry and Physics
Publication details, including instructions for authors and subscription information:
http://www.tandfonline.com/loi/tmph20

SiH_2, a critical study

Apostolos Kalemos [a b c], Thom H. Dunning Jr [a b c] & Aristides Mavridis [d]

[a] Joint Institute for Computational Sciences, University of Tennessee-Oak Ridge National Laboratory, Oak Ridge, Tennessee 37831, USA

[b] Department of Chemistry, University of Tennessee, Knoxville, Tennessee 37996, USA

[c] Computer Science and Mathematics Division, Oak Ridge National Laboratory, Oak Ridge, Tennessee 37831, USA

[d] Laboratory of Physical Chemistry, Department of Chemistry, National and Kapodistrian University of Athens, PO Box 64 004, 157 10 Zografou, Athens, Greece

[e] Joint Institute for Computational Sciences, University of Tennessee-Oak Ridge National Laboratory, Oak Ridge, Tennessee 37831, USA E-mail:

Published online: 21 Feb 2007.

To cite this article: Apostolos Kalemos, Thom H. Dunning Jr & Aristides Mavridis (2004) SiH_2, a critical study, Molecular Physics: An International Journal at the Interface Between Chemistry and Physics, 102:23-24, 2597-2606, DOI: 10.1080/00268970412331293802

To link to this article: http://dx.doi.org/10.1080/00268970412331293802

MOLECULAR PHYSICS, 10–20 DECEMBER 2004, VOL. 102, NO. 23–24, 2597–2606

SiH_2, a critical study

APOSTOLOS KALEMOS[1,2,3], THOM H. DUNNING JR[1,2,3*] and ARISTIDES MAVRIDIS[4]

[1]Joint Institute for Computational Sciences,
University of Tennessee-Oak Ridge National Laboratory,
Oak Ridge, Tennessee 37831, USA
[2]Department of Chemistry, University of Tennessee,
Knoxville, Tennessee 37996, USA
[3]Computer Science and Mathematics Division,
Oak Ridge National Laboratory, Oak Ridge, Tennessee 37831, USA
[4]Laboratory of Physical Chemistry, Department of Chemistry,
National and Kapodistrian University of Athens,
PO Box 64 004, 157 10 Zografou, Athens, Greece

(*Received 25 May 2004; accepted 4 August 2004*)

The first four spectroscopic states of the silylene molecule SiH_2, namely, $\tilde{X}^1A_1$, $\tilde{a}^3B_1$, $\tilde{A}^1B_1$ and $\tilde{B}^1A_1$ were examined theoretically using multireference methods coupled with very large correlation consistent basis sets. Our aim is understanding why SiH_2 has a singlet ground state ($\tilde{X}^1A_1$) as opposed to the $\tilde{X}^3B_1$ state of the isovalent carbene CH_2, as well as the rationalization of its geometric and bonding characteristics. The interpretational philosophy followed is based on strictly calculable quantities in an effort to reduce to a minimum the always present but not well-defined 'chemical intuitionism'. All of our calculated quantities are in excellent agreement with existing experimental results.

1. Introduction

'Why is methylene a ground state triplet while silylene is a ground state singlet?' is the title of a recently published article by Apeloig *et al*. [1] that tries to shed some light in the quite surprising reversal of the ground state multiplicities in going from CH_2 to SiH_2 based on a rather complicated energy decomposition scheme.

Along the same vein is the study by Gaspar *et al*. [2] entitled 'The quest for triplet ground state silylenes'. The authors believe that the larger size of the valence silicon orbitals in comparison with those of carbon is the main reason behind the elusiveness of the triplet ground state silylenes. They claim that the larger size of these orbitals leads to a decrease in the repulsion of the non-bonding electrons in the singlet state, hence their energy lowering separation in the triplet state is less capable of compensating an attendant promotion energy.

Influenced by Gordon [3], who as early as 1985 suggested that bulky substituents may open the angle in the singlet sufficiently to invert the ordering of the two states, Gaspar and collaborators [2] have been trying to synthesize such a substituted silylene hoping that the increased bond angle would reduce the energy difference between the in-plane and out-of-plane non-bonding orbitals, thus decreasing the promotion energy required to reach the triplet state. In 2001 Jiang and Gaspar [4] reported the end of a long quest for a triplet silylene based on the preparation of a product that could not arise from a singlet silylene at room temperature, and thus the reaction could be regarded as chemical evidence for its triplet ground state. Yoshida and Tamaoki [5], based on density functional theory (DFT) calculations over an extended range of substituted silylenes, suggested that the quest for a triplet ground state silylene must go on until a direct electron spin resonance (ESR) observation is recorded, a declaration also made by Gaspar *et al*. [2]. The quest is not finally over because of the lack of either an ESR signal or a chemically induced dynamic nuclear polarization nuclear magnetic resonance (NMR) experiment, or by detection of the silylene by kinetic ultraviolet (UV) spectroscopy.

It seems that the singlet ground state SiH_2 as opposed to the triplet ground state of the isovalent carbene, CH_2, is an afflictive question analogous to the distressing and rather troublesome issues that shaded for a long time the (correct) bent structure of the $\tilde{X}^3B_1$ state and $\tilde{a}^1A_1$–$\tilde{X}^3B_1$ splitting of the CH_2 molecule [6].

*Author for correspondence. e-mail: dunning@jics.utk.edu

Molecular Physics ISSN 0026–8976 print/ISSN 1362–3028 online © 2004 Taylor & Francis Ltd
http://www.tandf.co.uk/journals
DOI: 10.1080/00268970412331293802

The recent upsurge of interest in organosilicon chemistry coupled with the similarities and/or dissimilarities of the two archetypal CH_2 and SiH_2 molecules, have been the major motivation for research of both experimental and theoretical character. In particular, the challenging blend of Renner–Teller and spin–orbit couplings has been the focus of disentanglement studies of either spectroscopic or *ab initio* origin [7–47].

In our recent study of the first four electronic states of CH_2 [6], namely $\tilde{X}^3B_1$, $\tilde{a}^1A_1$, $\tilde{b}^1B_1$, and $\tilde{c}^1A_1$, we interpreted the geometrical and electronic structure of these states, in terms of the properties of its 'natural' constituents $CH + H(^2S)$. This was rather successful in rationalizing the bent structure of the $\tilde{X}^3B_1$ state, the quasi-linear configuration of the $\tilde{c}^1A_1$ state and the magnitude of the calculated inversion barriers. In the present study of the $\tilde{X}^1A_1$, $\tilde{a}^3B_1$, $\tilde{A}^1B_1$ and $\tilde{B}^1A_1$ states of SiH_2 an analysis—analogous to that performed in our previous CH_2 work—will be reported in order to better understand the physical reasons that lead to a ground singlet silylene state in contrast to the ground triplet state of the isovalent CH_2 molecule. Similarities and dissimilarities between these two molecules will be explained on the basis of the similarities and/or dissimilarities of their parental CH [48] and SiH [49] species. We believe that our interpretation based on *ab initio* methods and 'observable' quantum mechanical quantities offers a clear and convincing exposé of the SiH_2 properties exclusive of scientific battologies.

The existing experimental data pertaining to all known electronic states of SiH_2 are gathered in a recent compilation by Jacox [50] and can also be viewed in the chemistry Web book maintained by NIST [51]. The history and review of previous work is provided by several excellent reports recently published and will not be repeated in the current study [35, 36, 41, 43, 44, 47].

2. Methodological details

For the Si atom the aug-cc-pV6Z and the 'weighted' aug-cc-pwCV5Z basis sets of Dunning and co-workers, both generally contracted to [9s8p6d5f4g3h2i] and [12s11p9d7f5g3h], respectively, were employed [52]. The diffuse functions of the core-valence set were from the aug-cc-pV5Z basis set. For the H atom the plain cc-pV6Z ([6s5p4d3f2g1h]) basis set was used [53].

The standard internally contracted multireference CISD, as implemented in the MOLPRO package [54], based on a full valence (3s + 3p on Si and 1s on Hs) complete active space SCF reference wave function (CASSCF) was employed. The distribution of six valence electrons in the six valence orbitals generated CI reference expansions containing 56, 51, 39 and 56 configuration functions (CFs) for the $\tilde{X}^1A_1$, $\tilde{a}^3B_1$, $\tilde{A}^1B_1$ and $\tilde{B}^1A_1$ states, respectively. Additional correlation was taken into account by single and double replacements of either the six valence electrons, MRCI(6e$^-$), or the fourteen valence and core electrons (including the $2s^22p^6$ Si core electrons), MRCI(14e$^-$), out of the reference CASSCF wavefunctions.

For the first four states of SiH_2, i.e. the $\tilde{X}^1A_1$, $\tilde{a}^3B_1$, $\tilde{A}^1B_1$ and $\tilde{B}^1A_1$ states, and in analogy to the CH_2 molecule [6], two obvious formation channels can be considered, $Si + H_2SiH_2$ or $SiH + HSiH_2$. In detail

$$\begin{aligned} HSiH(^1\Delta_g) &\xrightarrow{C_{2v}} SiH_2(\tilde{X}^1A_1) \xrightarrow{C_{2v}} Si[\tfrac{1}{\sqrt{2}}(3p_x^2 - 3p_y^2); {}^1D] \\ &\quad + H_2(X^1\Sigma_g^+) \xrightarrow{C_{2v}} SiH_2(\tilde{A}^1B_1) \\ &\quad \xrightarrow{C_{2v}} Si(3p_z^1 3\overline{p}_x^1; {}^1D) + H_2(X^1\Sigma_g^+) \qquad (1\,a) \end{aligned}$$

$$\downarrow$$

$$\xrightarrow{C_{2v}} SiH(A^2\Delta) + H(^2S) \qquad (1\,b)$$

$$SiH_2(\tilde{a}^3B_1) \xrightarrow{C_{2v}} Si(3p_z^1 3p_x^1; {}^3P) + H_2(X^1\Sigma_g^+) \qquad (2\,a)$$

$$\downarrow$$

$$HSiH(^3\Sigma_g^-) \xrightarrow{C_{\infty v}} SiH(a^4\Sigma^-) + H(^2S) \qquad (2\,b)$$

$$\begin{aligned} SiH_2(\tilde{B}^1A_1) &\xrightarrow{C_{2v}} Si\{\tfrac{1}{\sqrt{6}}[2(3p_z^2) - 3p_x^2 - 3p_y^2]; {}^1D\} \\ &\quad + H_2(X^1\Sigma_g^+) \qquad (3\,a) \end{aligned}$$

$$\downarrow$$

$$HSiH(^1\Sigma_g^+) \xrightarrow{C_{\infty v}} SiH(C^2\Sigma^+) + H(^2S) \qquad (3\,b)$$

Two sets of fully optimized potential energy curves have been constructed at the valence–electron MRCI(6e$^-$) level; one along the bending coordinate HSiH = θ (equations (1 *a*), (2 *a*) and (3 *a*)) and a second one along the asymmetric dissociation mode, HSi + H (equations (1 *b*), (2 *b*) and (3 *b*)), figures 1 and 2, respectively. For the first set of curves, the SiH bond distance was optimized for each angle θ, for the second set of curves ($\theta = 180^\circ$) the HSi bond distances were optimized for each HSi–H separation.

3. Results and discussion

Table 1 lists the most recent and reliable theoretical and experimental results from the literature on the first four SiH_2 states, table 2 displays the Si atomic energies of several valence and Rydberg states at the MRCI(4e$^-$) and MRCI(12e$^-$) level, table 3 presents results on the $X^2\Pi$, $a^4\Sigma^-$, $A^2\Delta$, $B^2\Sigma^-$ and $C^2\Sigma^+$ SiH states pertaining to the present study at different levels of theory, while table 4 lists results on the SiH_2 states studied

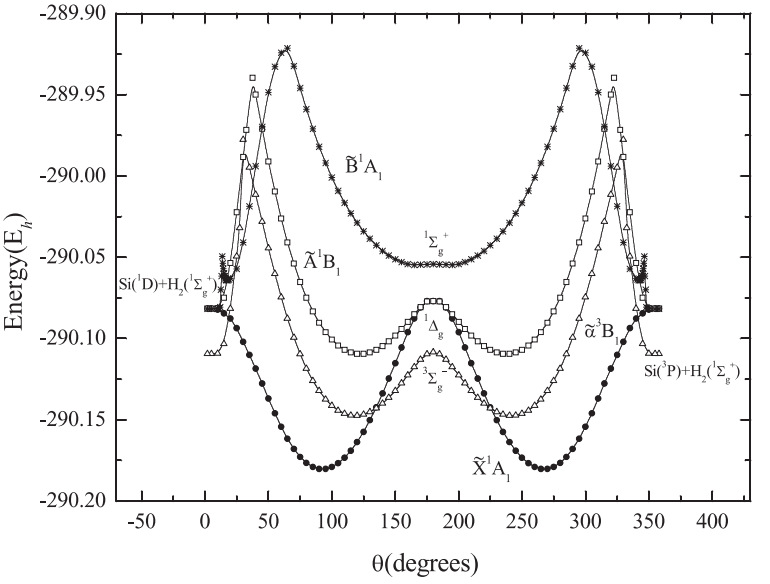

Figure 1. Potential energy profiles of the $\tilde{X}^1A_1$, $\tilde{a}^3B_1$, $\tilde{A}^1B_1$ and $\tilde{B}^1A_1$ SiH_2 states at the MRCI($6e^-$) level along the HSiH bending mode.

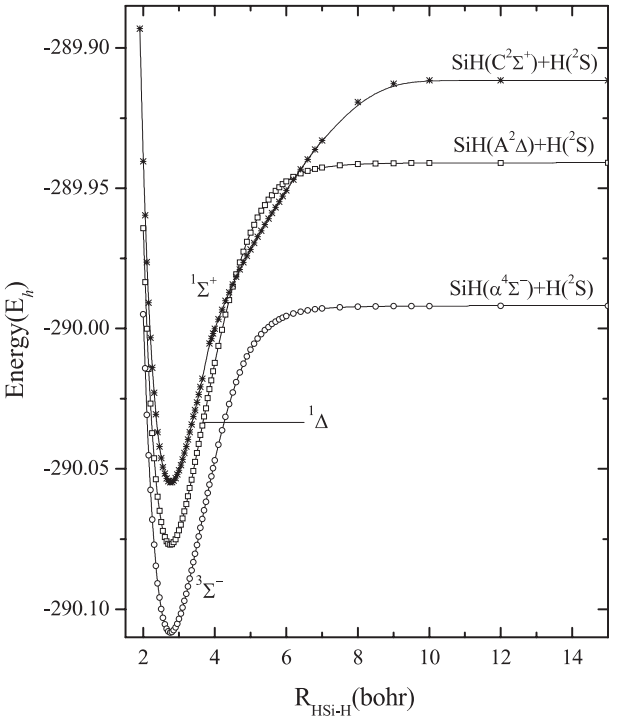

Figure 2. Potential energy profiles of the HSi + H along the $\mathcal{C}_{\infty v}$ dissociation channel at the MRCI($6e^-$) level.

in the current work. Figures 1 and 2 depict potential energy curves with respect to θ (equations (1*a*), (2*a*) and (3*a*)) and to the HSiH→HSi + H dissociation channel (equations (1*b*), (2*b*) and (3*b*)), figure 3 is a relative energy level diagram of the isovalent species CH and SiH at the MRCI level of theory, and figures 4 and 5 display the energy stabilization along the HC→HCH→CH_2 and HSi→HSiH→SiH_2 routes, respectively.

3.1. $\tilde{X}^1A_1$

The leading CASSCF configurations of the ground SiH_2 state are (only valence electrons are counted) $|\tilde{X}^1A_1\rangle \sim |1a_1^2[0.97(2a_1^2) - 0.22(1b_1^2)]1b_2^2\rangle$, identical to those of the $\tilde{a}^1A_1$ CH_2 state [6]. At $\theta = 180^\circ$ the $\tilde{X}^1A_1$ correlates with the linear $^1\Delta_g$ symmetry, figure 1, which along the asymmetric dissociation mode ($\mathcal{C}_{\infty v}$) correlates to the $A^2\Delta$ SiH state (figure 2). The bent $^1A_1$ structure dissociates, along C_s, to the $X^2\Pi$ SiH state, 70.33 kcal mol^{-1} below the $A^2\Delta$ state; see table 3. Pictorially, the $X^2\Pi$ and $A^2\Delta$ SiH states are represented by the following valence-bond Lewis (vbL) diagrams

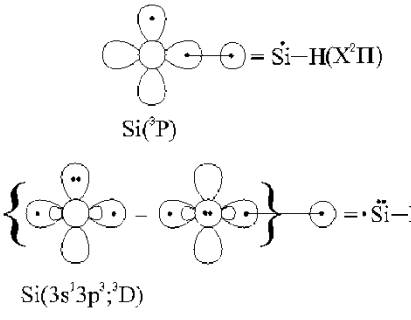

Table 1. Best theoretical and experimental results on the $\tilde{X}^1A_1$, $\tilde{a}^3B_1$, $\tilde{A}^1B_1$ and $\tilde{B}^1A_1$ states of SiH_2. Total energies E(hartree), bond distances r_e(Å), HSiH angles θ_e(degrees), zero point energies ZPE(cm^{-1}), and energy gaps T_e/T_0(kcal mol^{-1}).

$-E$	r_e	θ_e	ZPE	T_e/T_0	Ref./Year
$\tilde{X}^1A_1$					
290.164347[a]	1.5124	92.74	2619.5	0.0	41/1997
290.168206[b]	1.5124	92.74		0.0	41/1997
290.170278[c]	1.5124	92.74		0.0	41/1997
290.16586[d]	1.542	93.9	2467.5	0.0	38/1994
290.1757118[e]	1.5168	92.04	2543.0	0.0	36/1993
	(1.5180)[f]	(92.15)[f]			36/1993
290.181186[g]	1.51477	92.42		0.0	33/1992
290.179379[h]	1.51477	92.42		0.0	33/1992
290.489407[i]	1.51477	92.42		0.0	33/1992
290.177661[j]	1.519	92.5		0.0	24/1987
Expt.[k]	1.51402	91.9830		0.0	43/1998
Expt.[l]	[1.525(6)]	[91.8(10)]		0.0	27/1989
	1.5140	92.08		0.0	27/1989
Expt.[m]	[1.516_3]	[92.8]		0.0	9/1968
Expt.[n]	1.5141	92.0		0.0	20/1986
$\tilde{a}^3B_1$					
290.131803[a]	1.4760	118.24	2719.5	20.42/20.71	41/1997
290.136337[b]	1.4760	118.24		20.00/20.29	41/1997
290.138047[c]	1.4760	118.24		20.23/20.52	41/1997
290.13482[d]	1.501	117.8	2572.5	19.48/19.78	38/1994
290.1440123[e]	1.4793	118.426	2676.2	19.89/20.27	36/1993
	(1.4788)[f]	(125.862)[f]			36/1993
290.148862[g]	1.47681	118.30		20.28	33/1992
290.147102[h]	1.47681	118.30		20.25	33/1992
290.456426[i]	1.47681	118.30		20.70	33/1992
290.145322[j]	1.483	118.3		20.29/20.9[o]	24/1987
Expt.[p]				20.99 ± 0.69	21/1987
$\tilde{A}^1B_1$					
290.091085[a]	1.4814	122.87	2650.5	45.97/46.06	41/1997
290.097085[b]	1.4814	122.87		44.63/44.72	41/1997
290.098518[c]	1.4814	122.87		45.03/45.12	41/1997
Expt.[k]	1.48532	122.4416		44.453	43/1998
Expt.[q]				44.403 ± 0.0014	34/1993
Expt.[m]	[1.48_7]	[123]		44.41	9/1968
Expt.[n]	1.4871	121.83			20/1986
$\tilde{B}^1A_1$					
290.033682[a]	1.4577	162.27	2783	81.99/82.46	41/1997
290.042235[b]	1.4577	162.27		79.05/79.52	41/1997
290.044159[c]	1.4577	162.27		79.14/79.61	41/1997

[a]CISD/[8s7p3d2f/5s3p2d] with the highest–lying virtual orbital deleted. ZPE based on harmonic frequencies.
[b]CASSCF($6e^-$/6 orbitals) + 1 + 2/TZ3P(2f,2d)//CISD/TZ3P(2f,2d).
[c]CASSCF($6e^-$/8 orbitals) + 1 + 2/TZ3P(2f,2d) + 2diff//CISD/TZ3P(2f,2d) + 2diff.
[d]MRCI + Q/cc−pVTZ(−f)//CASSCF/cc−pVTZ(−f). ZPE based on harmonic frequencies at the CASSCF/cc−pVTZ(−f) level of theory.
[e]The energy corresponds to the C_{000} value of a polynomial expansion that fits CEPA/[11s8p4d2f/4s3p1d] energy points around equilibrium.
[f]r_0 and θ_0 values.
[g]CCSD(T)/[6s5p3d2f1g/4s3p2d1f]//CISD/[6s5p2d/4s2p].
[h]CCSD(T)/[7s7p7d6f/4s2p1d]//CISD/[6s5p2d/4s2p].
[i]CCSD(T)/[7s7p7d6f/4s2p1d]//CISD/[6s5p2d/4s2p], the core electrons [Si($\sim 2s^2 2p^6$)] are included in the correlation treatment.
[j]MRCI/[6s5p3d2f1g/4s3p2d].
[k]Laser absorption spectroscopy; the rotational constants at equilibrium were calculated using the theoretically derived rovibrational constants α_i^B from [20].

Table 2. Total energies E(hartree) of the $^3P(3s^23p^2)$, $^1D(3s^23p^2)$, $^1S(3s^23p^2)$, $^5S(3s^13p^3)$, $^3P(3s^23p^14s^1)$, and $^1P(3s^23p^14s^1)$ Si states and corresponding energy gaps ΔE(eV) with respect to the ground states at the MRCI level of theory.

$^3P(3s^23p^2)$	$^1D(3s^23p^2)$	$^1S(3s^23p^2)$	$^5S(3s^13p^3)$	$^3P(3s^23p^14s^1)$	$^1P(3s^23p^14s^1)$
−288.936653[a]	−288.909380	−288.868015	−288.794111	−288.755868	−288.750280
−288.936445[b]	−288.909101	−288.867684	−288.794003	−288.755420	−288.749727
−289.241820[c]	−289.211651	−289.172930	−289.103434	−289.063488	−289.057005
	$^1D \leftarrow {}^3P$	$^1S \leftarrow {}^3P$	$^5S \leftarrow {}^3P$	$^3P \leftarrow {}^3P$	$^1P \leftarrow {}^3P$
	0.742[a]	1.868	3.879	4.919	5.071
	0.744[b]	1.871	3.876	4.926	5.081
	0.821[c]	1.875	3.766	4.853	5.029
Expt.[d]	0.762	1.890	4.113	4.923	5.064

[a]MRCI(4e$^-$)/aug−cc−pV6Z.
[b]MRCI(4e$^-$)/aug−cc−pwCV5Z.
[c]MRCI(12e$^-$)/aug−cc−pwCV5Z.
[d][55].

A linear and perpendicular H-attack on the $A^2\Delta$ and $X^2\Pi$ SiH states, respectively, results in the $^1\Delta_g$ ($\theta = 180^\circ$) and $^1A_1(\theta = 90^\circ)$ configurations of SiH_2, or in vbL graphical language

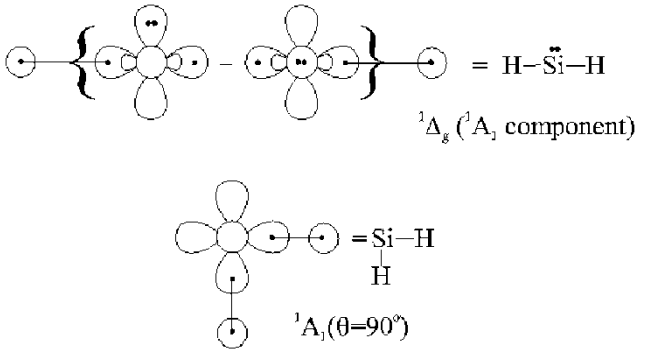

Figure 5 shows the energy profile of the whole process, i.e., $HSi(A^2\Delta) + H(^2S) \rightarrow HSiH(^1\Delta_g) \rightarrow SiH_2(\tilde{X}^1A_1)$. The dissociation energy HSi–H of the $^1\Delta_g$ structure, along the $\mathcal{C}_{\infty v}$ pathway, is $D_e = 85.37\,\text{kcal mol}^{-1}$ at the MRCI(6e$^-$) level of theory (see also figure 2), while the inversion barrier $IB_e[HSiH(^1\Delta_g) \leftarrow SiH_2(\tilde{X}^1A_1)] = 64.85\,\text{kcal mol}^{-1}$ (table 4). The $\tilde{X}^1A_1$ SiH_2 state is stabilized by $85.37 + 64.85 = 150.22\,\text{kcal mol}^{-1}$ with respect to $HSi(A^2\Delta) + H(^2S)$. In the $^1A_1(\theta = 90^\circ)$ structure the (HSi)–H bond energy is $79.80\,\text{kcal mol}^{-1}$ with respect to $HSi(X^2\Pi) + H(^2S)$.

In the CH_2 molecule the analogous reaction channels are $HC(A^2\Delta) + H(^2S) \rightarrow HCH(^1\Delta_g) \rightarrow CH_2(\tilde{a}^1A_1)$, $\Delta E_e = 137.77 + 26.35 = 164.12\,\text{kcal mol}^{-1}$, and CH_2 $[^1A_1(\theta = 90^\circ)] \rightarrow HC(X^2\Pi) + H(^2S)$, $D_e = 94.42\,\text{kcal mol}^{-1}$, at the all-electron MRCI level of theory (figure 4) [6]. The energy difference between the two limiting structures, $^1A_1(\theta = 90^\circ)$ and $^1\Delta_g(\theta = 180^\circ)$ is only $24.12\,\text{kcal mol}^{-1}$ as contrasted to the much higher value of $64.76\,\text{kcal mol}^{-1}$ in the SiH_2 molecule. This results in a stronger pseudo Jahn–Teller vibronic interaction between these two limiting structures in the CH_2 case with a final HCH angle of $\theta_e = 102.20^\circ$, while in SiH_2 the much more stable $^1A_1(\theta = 90^\circ)$ structure does not interact with the linear one, therefore the resulting $\tilde{X}$-state has a final angle $\theta_e = 92.52^\circ$ (table 4), very close to the geometry of the 'perpendicular' limiting structure.

The $\tilde{X}^1A_1$ state smoothly dissociates to $Si(^1D) + H_2(X^1\Sigma_g^+)$ (equation (1 *a*)) as evidenced in figure 1, with no insertion barrier. The same also holds true in the isovalent CH_2 $\tilde{a}^1A_1$ state [6]. The reason for this barrierless reaction is attributed to the electronic configuration of the Si atom with its $|^1D; 1/2^{1/2}(3p_x^2 - 3p_y^2)\rangle$ distribution. No electronic density along the $\mathcal{C}_{2v}$ (z) axis hinders the incoming $^1\Sigma_g^+$ H_2-distribution as opposed to the $^3B_1$, $^1B_1$ and $(\tilde{B})^1A_1$ symmetries, figure 1. The size extensivity error is 2.16 (1.66) mhartree at the MRCI(+Davidson correction = +Q) level of theory.

[l]Infrared diode laser kinetic spectroscopy; values in brackets correspond to r_0 and θ_0 values, the r_e and θ_e values were estimated by referring to the vibration−rotation constants of the H_2S molecule.
[m]r_0 and θ_0 values.
[n]The rotational constants from [9] and theoretical rovibrational constants were used to extract the equilibrium values.
[o]ZPE correction ($+0.33\,\text{kcal mol}^{-1}$) and relativistic effects ($+0.3\,\text{kcal mol}^{-1}$) are included.
[p]Photoionization mass spectroscopy.
[q]Laser-induced fluorescence.

Table 3. Total energies E(hartree), dissociation energies D_e(kcal mol^{-1}), bond distances r_e(Å), dipole moments $\mu_e(D)$, and energy separations T_e(kcal mol^{-1}) of the $X^2\Pi$, $a^4\Sigma^-$, $A^2\Delta$, $B^2\Sigma^-$ and $C^2\Sigma^+$ states of the SiH molecular system. Present work.

State	$-E$	D_e[a]	r_e	μ_e[b]	T_e
$X^2\Pi$	289.553 039[c]	73.02	1.5233	0.1476	0.0
	289.552 856[d]	73.04	1.5229	0.1466	0.0
	289.857 096[e]	72.34	1.5190	0.2331	0.0
	289.557 373[f]	73.55	1.5223	0.124	0.0
	Expt.[g]	72.35−73.46	1.51966_7		0.0
$a^4\Sigma^-$	289.491 937[c]	34.52	1.4941	−0.0047	38.34
	289.491 779[d]	34.59	1.4937	−0.0047	38.33
	289.797 627[e]	34.78	1.4820	−0.0221	37.32
	289.495 594[f]	34.73	1.4974	−0.027	38.77
$A^2\Delta$	289.440 965[c]	20.11	1.5277	0.1083	70.33
	289.440 716[d]	20.12	1.5272	0.1076	70.37
	289.740 767[e]	18.03	1.5261	0.1816	73.00
	289.447 424[f]	22.28	1.5240	0.098	68.99
	Expt.[g]	20.58–21.69	1.5197816_{21}		69.35
$B^2\Sigma^-$	289.437 079[c]	0.13	3.5778	0.0558	72.77
	289.436 868[d]	0.13	3.5772	0.0561	72.78
	289.742 326[e]	0.08	3.8653	0.0528	72.02
	289.440 547[f]	0.19	3.440	0.093	73.31
	Expt.[h]				73.31–76.24
local minimum					
	289.435 763[c]		1.7240	0.6351	
	289.435 501[d]		1.7236	0.6340	
	289.740 640[e]		1.7215	0.7083	
	289.439 778[f]		1.7154	0.621	
$C^2\Sigma^+$	289.411 502[c]	1.09	1.5342	0.1579	88.82
	289.411 219[d]	2.53	1.5336	0.1572	88.88
	289.712 908[e]	4.34	1.5378	0.2580	90.48
	289.416 551[f]	2.89	1.5338	0.178	88.37
local minimum					
	289.410 595[e]		2.7001	−0.7300	
	289.407 810[d]		2.6222	−1.021	
	289.705 560[e]		2.2756	−1.717	
	289.414 926[f]		2.40	−1.245	

[a] D_e with respect to the adiabatic products.
[b] Calculated as expectation value.
[c] MRCI(6e$^-$)/[aug−cc−pV6Z/cc−pV6Z].
[d] MRCI(6e$^-$)/[aug−cc−pwCV5Z/cc−pV6Z].
[e] MRCI(14e$^-$)/[aug−cc−pwCV5Z/cc−pV6Z].
[f] [49].
[g] r_e from [56] and D_e from [57].
[h] [57].

3.2. $\tilde{a}^3B_1$

The prevailing CASSCF equilibrium configuration is $|\tilde{a}^3B_1\rangle \sim 0.99|1a_1^2 2a_1^1 1b_1^1 1b_2^2\rangle$, identical to that for the isovalent CH_2 $\tilde{X}^3B_1$ state. At linearity ($\theta = 180°$) it correlates to a $^3\Sigma_g^-$ symmetry configuration which dissociates to $HSi(a^4\Sigma^-) + H(^2S)$; see figure 2. The vbL icon of the generic $a^4\Sigma^-$ state is [49]

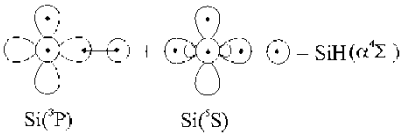

Two modes of H-attack are obvious, a linear one resulting in the linear $^3\Sigma_g^-(\theta = 180°)$ structure and a perpendicular one giving rise to a bent $^3B_1(\theta = 90°)$ structure 15.06 kcal mol^{-1} below the linear structure; see figures 1 and 5. In the CH_2 molecule the pseudo Jahn–Teller vibronic interaction of these two limiting structures results in the $\tilde{X}^3B_1$ state while in the isovalent SiH_2 system the analogous interaction gives rise to the first excited $\tilde{a}^3B_1$ state lying 20.68 kcal mol^{-1} above the $\tilde{X}^1A_1$ state (table 4).

The long-standing question of this spin reversal of $\tilde{X}^3B_1(CH_2)$ vs $\tilde{X}^1A_1(SiH_2)$, can be elucidated by con-

Table 4. Total energies E(hartree), bond distances r_e(Å), HSiH angles θ_e(degrees), dipole moments μ_e(D), inversion barriers IB$_e$(kcal mol^{-1}), atomization energies AE$_e$(kcal mol^{-1}), and energy gaps T_e(kcal mol^{-1}) of the $\tilde{X}^1A_1$, $\tilde{a}^3B_1$, $\tilde{A}^1B_1$, and $\tilde{B}^1A_1$ states of SiH_2. Present work.

$-E$	r_e	θ_e	μ_e[a]	IB$_e$	AE$_e$[b]	T_e
$\tilde{X}^1A_1$						
290.180 368[c]	1.5171	92.52	0.1674	64.85[d]	152.93	0.0
290.180 235[e]	1.5167	92.52	0.1666		152.98	0.0
290.485 827[f]	1.5112	92.84	0.2148		153.12	0.0
$\tilde{a}^3B_1$						
290.147 417[c]	1.4760	118.24	−0.0208	24.57[g]	132.26	20.68
290.147 301[e]	1.4799	118.21	−0.0246		132.31	20.67
290.452 655[f]	1.4735	118.25	0.0163		132.30	20.82
$\tilde{A}^1B_1$						
290.109 491[c]	1.4890	122.26	0.0087	20.38[d]	108.46	44.48
290.109 305[e]	1.4886	122.25	0.0077		108.47	44.51
290.414 110[f]	1.4839	121.68	0.0291		108.11	45.00
$\tilde{B}^1A_1$						
290.055 713[c]	1.4577	162.20	−0.0776	0.99[h]	74.71	78.22
290.055 654[e]	1.4652	165.60	−0.0129		74.80	78.18
290.353 541[f]	1.4551	167.62	0.2895		70.11	83.01

[a]Calculated as expectation value.
[b]With respect to Si(^{3}P) + 2H(^{2}S).
[c]MRCI(6e$^-$)/[aug−cc−pV6Z/cc−pV6Z].
[d]At $r_e(^1\Delta_g) = 1.4570$ Å, $E(^1\Delta_g) = -290.077\,017$ hartree.
[e]MRCI(6e$^-$)/[aug−cc−pwCV5Z/cc−pV6Z]
[f]MRCI(14e$^-$)/[aug−cc−pwCV5Z/cc−V6Z].
[g]At $r_e(^3\Sigma_g^-) = 1.4603$ Å, $E = -290.108\,270$ hartree.
[h]At $r_e(^1\Sigma_g^+) = 1.4638$ Å, $E = -290.054\,135$ hartree.

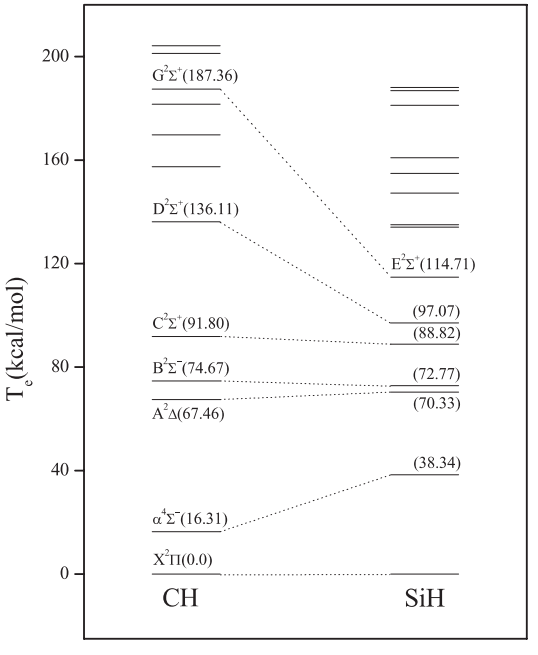

Figure 3. Relative energy levels of the isovalent CH and SiH species at the MRCI level of theory. Dotted lines connect similar states of the two species.

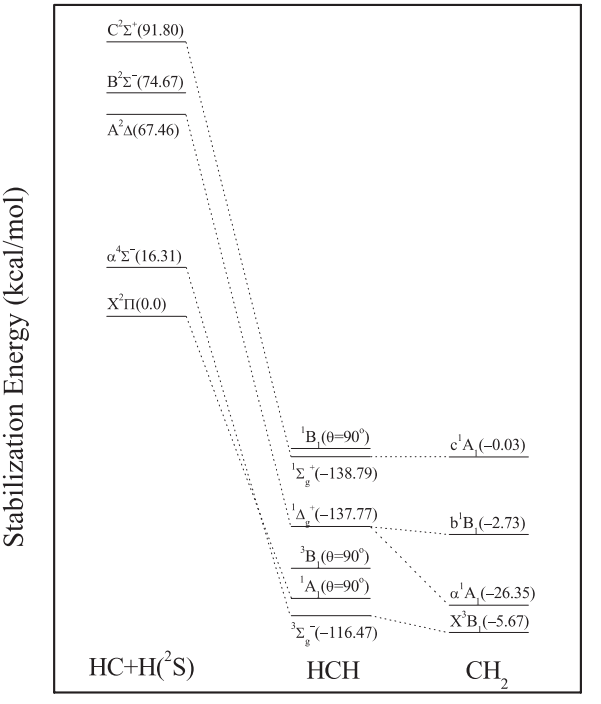

Figure 4. Energy stabilization along the HC + H → HCH → CH_2 route at the all-electron MRCI level of theory.

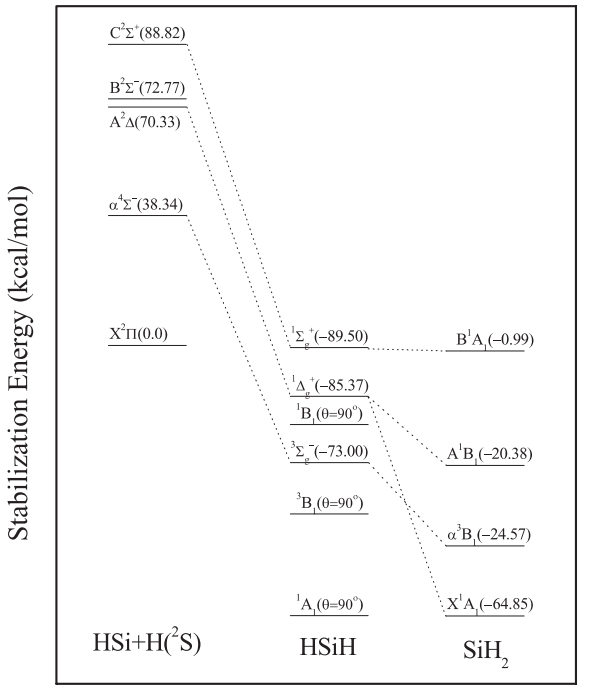

Figure 5. Energy stabilization along the $HSi + H \rightarrow HSiH \rightarrow SiH_2$ route at the MRCI($6e^-$) level of theory.

sidering the evolution from the constituent fragments to the end products. In the CH_2 case this process is captured in detail in figure 4, i.e. $HC(a^4\Sigma^-) + H(^2S) \rightarrow HCH(^3\Sigma_g^-) \rightarrow CH_2(\tilde{X}^3B_1)$, with a stabilization energy of $116.47 + 5.67 = 122.14\,kcal\,mol^{-1}$ with respect to $HC(a^4\Sigma^-) + H(^2S)$, or $122.14 - T_e(a^4\Sigma^- \leftarrow X^2\Pi) = 122.14 - 16.31 = 105.83\,kcal\,mol^{-1}$ with respect to the ground state products. The $\tilde{a}^1A_1$ state is $96.59\,kcal\,mol^{-1}$ below the $CH(X^2\Pi) + H(^2S)$ level resulting in an energy gap $T_e(CH_2;\ \tilde{a}^1A_1 \leftarrow \tilde{X}^3B_1) = 9.24\,kcal\,mol^{-1}$ [6]. The energy profile of the analogous process in the SiH_2 case is depicted in figure 5. The binding energy of the $HSiH(^3\Sigma_g^-)$ structure with respect to $HSi(a^4\Sigma^-) + H(^2S)$ limit is $D_e = 73.00\,kcal\,mol^{-1}$ and the $IB_e(^3\Sigma_g^- \leftarrow \tilde{a}^3B_1) = 24.57\,kcal\,mol^{-1}$. With respect to the ground state fragments, $SiH(X^2\Pi) + H(^2S)$, the $\tilde{a}^3B_1$ state is stabilized by $D_e + IB_e - T_e(a^4\Sigma^- \leftarrow X^2\Pi) = 73.00 + 24.57 - 38.34 = 59.23\,kcal\,mol^{-1}$ and the $\tilde{X}^1A_1$ state by $79.91\,kcal\,mol^{-1}$. The key quantity in understanding the reason for the spin reversal of the ground state of CH_2 and SiH_2 is the $T_e(SiH; a^4\Sigma^- \leftarrow X^2\Pi) = 38.34\,kcal\,mol^{-1}$ as contrasted to the much smaller $T_e(CH; a^4\Sigma^- \leftarrow X^2\Pi) = 16.31\,kcal\,mol^{-1}$. Lowering the $HSi(a^4\Sigma^-) + H(^2S) \rightarrow HSiH(^3\Sigma_g^-) \rightarrow SiH_2(\tilde{a}^3B_1)$ process by $T_e(SiH; a^4\Sigma^- \leftarrow X^2\Pi) - T_e(CH; a^4\Sigma^- \leftarrow X^2\Pi) = 38.34 - 16.31 = 22.03\,kcal\,mol^{-1}$ we get a $\tilde{X}^3B_1$ SiH_2 state with the $\tilde{a}^1A_1$ state differing in energy by $22.03 - 20.68 = 1.35\,kcal\,mol^{-1}$.

In further support of this reasoning, we report the rather high energy gap $T_e(\tilde{a}^1A_1 \leftarrow \tilde{X}^3B_1) = 28.97\,kcal\,mol^{-1}$ of the NH_2^+ molecule [58] (isoelectronic to CH_2) and the $T_e(\tilde{a}^3B_1 \leftarrow \tilde{X}^1A_1) = 18.94\,kcal\,mol^{-1}$ of the PH_2^+ molecule [59] (isoelectronic to SiH_2). In the NH_2^+ case the rather large energy gap between the ground triplet and first excited singlet states can be attributed to the quasi degenerate $a^4\Sigma^-$ and $X^2\Pi$ NH^+ states, $T_e(NH^+; a^4\Sigma^- \leftarrow X^2\Pi) = 500\,cm^{-1} (= 1.43\,kcal\,mol^{-1})$ [60], while a $T_e(PH^+; a^4\Sigma^- \leftarrow X^2\Pi) = 1.64\,eV\ (= 37.82\,kcal\,mol^{-1})$ is reported for the PH^+ system [61].

An energy barrier of $82.6\,kcal\,mol^{-1}$ accompanies the $Si(^3P; 3p_z 3p_x) + H_2(^1\Sigma_g^+)$ insertion (figure 1), while our calculations suffer by a size extensivity error of 1.67(0.31) mhartree at the MRCI(+Q) level of theory.

3.3. $\tilde{A}^1B_1$

The open shell singlet analogue of the previously discussed $\tilde{a}^3B_1$ state is dominated by the CASSCF configuration, $|\tilde{A}^1B_1\rangle \sim 0.98|1a_1^2 2a_1^1 1\bar{b}_1^1 1b_2^2\rangle$. At linearity it becomes the Renner–Teller companion of the $\tilde{X}^1A_1$ state with a splitting that becomes noticeable at rather large θ values; see figure 1. The $A^2\Delta$ and $B^2\Sigma^-$ SiH states can be considered as parental for the current SiH_2 state:

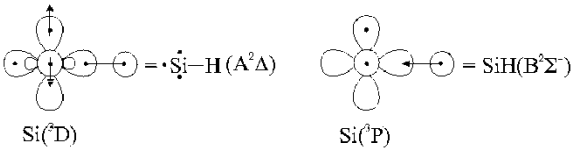

In line with our previous discussion, a linear H-attack on the $A^2\Delta$ state and a perpendicular H-attack on the $B^2\Sigma^-$ state give the $^1\Delta_g(\theta = 180^\circ)$ and $^1B_1(\theta = 90^\circ)$ SiH_2 structures differing in energy by $8.31\,kcal\,mol^{-1}$; see figure 5. The interaction of these two structures results in the $\tilde{A}^1B_1$ state with $\theta_e = 122.26^\circ$. The energetic and geometric features are in excellent agreement with the existing experimental results (tables 1 and 4). The reaction $Si(3p_z^1 3\bar{p}_x^1; {}^1D) + H_2(X^1\Sigma_g^+)$ proceeds with an energy barrier of $89.10\,kcal\,mol^{-1}$ while the energy of the supermolecule is higher than the sum of the energies of the reactive species by 2.16(1.67) mhartree at the MRCI(+Q) level of theory.

3.4. $\tilde{B}^1A_1$

The last studied SiH_2 state is in every respect similar to the $\tilde{c}^1A_1$ CH_2 state [6]. With an angle $\theta_e = 162.2^\circ$ and an $IB_e(^1\Sigma_g^+ \leftarrow \tilde{B}^1A_1) = 0.99\,kcal\,mol^{-1}$ (table 4), it is essentially (vibrationally) linear. The leading CASSCF

configurations

$$\left|\tilde{\mathbf{B}}^1\mathrm{A}_1\right\rangle \sim 0.83\left|1a_1^2 1b_1^2 1b_2^2\right\rangle + 0.48\left|1a_1^2 2a_1^2 1b_2^2\right\rangle - 0.22\left|1a_1^2 3a_1^2 1b_2^2\right\rangle$$

carry the memory of the dissociation limit $SiH(C^2\Sigma^+)$; see figure 2. Its practical linearity, as in the $\tilde{c}^1A_1$ CH_2 state, results from the absence of any other SiH state that could bend substantially the final geometry. The $D^2\Sigma^+$ SiH state, although only 8.3 kcal mol^{-1} above the $C^2\Sigma^+$, offers no alternative H-attack (as is the case for the previously discussed states). The dissociation curve of figure 2 is eloquently described graphically by the following vbL icons providing also an explanation for its floppiness.

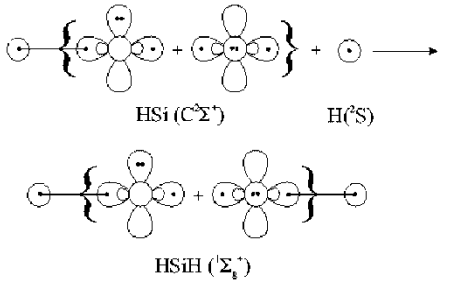

4. Conclusions

In line with our previous study on CH [48], CH_2 [6] and SiH [49], we present state-of-the-art *ab initio* calculations on the first four SiH_2 states, i.e. the $\tilde{X}^1A_1$, $\tilde{a}^3B_1$, $\tilde{A}^1B_1$ and $\tilde{B}^1A_1$ states. Multireference methods coupled with large basis sets were employed for the construction of potential energy curves along the bending and asymmetric dissociation modes, figures 1 and 2, respectively. The existing experimental data are in excellent agreement with the results presented herein (tables 1 and 4). The geometrical features and bonding characteristics of the states examined are interpreted by correlating the SiH_2 states with their parental SiH states, while similarities and/or dissimilarities between CH_2 and SiH_2 can also be explained on the basis of their parental CH and SiH species.

By analysing the $XH + H \rightarrow XH_2$ pathways for X = C and Si, it was found that a key quantity in understanding the reason for the spin reversal of the ground state of CH_2 and SiH_2 is the difference in the $a^4\Sigma^- \leftarrow X^2\Pi$ excitation energies for SiH and CH, $T_e(SiH) = 38.34$ kcal mol^{-1} as contrasted to the much smaller $T_e(CH) = 16.31$ kcal mol^{-1}. The $\tilde{X}^3B_1$ state in CH_2 is stabilized by 122.14 kcal mol^{-1} relative to the $a^4\Sigma^-$ state of CH; in SiH_2 the stabilization is 97.57 kcal mol^{-1}. The $\tilde{a}^1A_1$ state in CH_2 is stabilized by 96.66 kcal mol^{-1} relative to the $X^2\Pi$ state of CH; in SiH_2 the stabilization is 76.89 kcal mol^{-1}. Although the magnitudes of the stabilization energies in CH_2 and SiH_2 differ significantly, the differences in the stabilization energies for the $^3B_1$ and $^1A_1$ states are similar: 25.55 kcal mol^{-1} in CH_2 and 17.66 kcal mol^{-1} in SiH_2. These differences are comparable to the difference in $T_e(a^4\Sigma^- \leftarrow X^2\Pi)$, 22.03 kcal mol^{-1} and is sufficient to reverse the order of the $^3B_1$ and $^1A_1$ states in SiH_2.

This work was performed in part at the Joint Institute for Computational Sciences, University of Tennessee–Oak Ridge National Laboratory. Support was provided by the Distinguished Scientist Program at the University of Tennessee and Oak Ridge National Laboratory. Oak Ridge National Laboratory is managed by UT-Battelle, LLC for the US Department of Energy under Contract No. DE-AC05-00OR22725.

References

[1] Apeloig, Y., Pauncz, R., Karni, M., West, R., Steiner, W., and Chapman, D., 2003, *Organometallics*, **22,** 3250.
[2] Gaspar, P. P., Xiao, M., Pae, D. H., Berger, D. J., Haile, T., Chen, T., Lei, D., Winchester, W. R., and Jiang, P., 2002, *J. Organometallic Chem.*, **646,** 68.
[3] Gordon, M. S., 1985, *Chem. Phys. Lett.*, **114,** 348.
[4] Jiang, P., and Gaspar, P. P., 2001, *J. Am. Chem. Soc.*, **123,** 8622; see also 2001, *Chem. Eng. News*, **79**(37), 29.
[5] Yoshida, M., and Tamaoki, N., 2002, *Organometallics*, **21,** 2587.
[6] See for example Kalemos, A., Dunning Jr, T. H., Mavridis, A., and Harrison, J. F., 2004, *Can. J. Chem.*, **82,** 684.
[7] Jordan, P. C., 1966, *J. Chem. Phys.*, **44,** 3400.
[8] Dubois, I., Herzberg, G., and Verma, R. D., 1967, *J. Chem. Phys.*, **47,** 4262.
[9] Dubois, I., 1968, *Can. J. Phys.*, **46,** 2485.
[10] Milligan, D. E., and Jacox, M. E., 1970, *J. Chem. Phys.*, **52,** 2594.
[11] Wirsam, B., 1972, *Chem. Phys. Lett.*, **14,** 214.
[12] Dubois, I., Duxbury, G., and Dixon, R. N., 1975, *J. Chem. Soc. Faraday Trans. II*, **71,** 799.
[13] Kasdan, A., Herbst, E., and Lineberger, W. C., 1975, *J. Chem. Phys.*, **62,** 541.
[14] Meadows, J. H., and Schaefer III, H. F., 1976, *J. Am. Chem. Soc.*, **98,** 4383.
[15] Sauer, J., Čársky, P., and Zahradnik, R., 1982, *Collect. Czech. Chem. Commun.*, **47,** 1149.
[16] Colvin, M. E., Grev, R. S., Schaefer III, H. F., and Bicerano, J. C., 1983, *Chem. Phys. Lett.*, **99,** 399.
[17] Rice, J. E., and Handy, N. C., 1984, *Chem. Phys. Lett.*, **107,** 365.
[18] Fredin, L., Hauge, R. H., Kafafi, Z. H., and Margrave, J. L., 1985, *J. Chem. Phys.*, **82,** 3542.
[19] Balasubramanian, K., and McLean, A. D., 1986, *J. Chem. Phys.*, **85,** 5117.
[20] Allen, W. D., and Schaefer III, H. F., 1986, *Chem. Phys.*, **108,** 243 and references cited therein.
[21] Berkowitz, J., Greene, J. P., Cho, H., and Ruscic, B., 1987, *J. Chem. Phys.*, **86,** 1235.

[22] Bauschlicher Jr, C. W., and Taylor, P. R., 1987, *J. Chem. Phys.*, **86,** 1420.
[23] Bauschlicher Jr, C. W., and Taylor, P. R., 1987, *J. Chem. Phys.*, **86,** 2844.
[24] Bauschlicher Jr, C. W., Langhoff, S. R., and Taylor, P. R., 1987, *J. Chem. Phys.*, **87,** 387.
[25] Francisco, J. S., Barnes, R., and Thoman Jr, J. W., 1988, *J. Chem. Phys.*, **88,** 2334.
[26] Selmani, A., and Salahub, D. R., 1988, *J. Chem. Phys.*, **89,** 1529.
[27] Yamada, C., Kanamori, H., Hirota, E., Nishiwaki, N., Itabashi, N., Kato, K., and Goto, T., 1989, *J. Chem. Phys.*, **91,** 4582.
[28] Shin, S. K., Goddard III, W. A., and Beauchamp, J. L., 1990, *J. Chem. Phys.*, **93,** 4986.
[29] McKay, R. I., Uichanco, A. S., Bradley, A. J., Holdsworth, J. R., Francisco, J. S., Steinfeld, J. I., and Knight, A. E. W., 1991, *J. Chem. Phys.*, **95,** 1688.
[30] Ishikawa, H., and Kajimoto, O., 1991, *J. Molec. Spectrosc.*, **150,** 610.
[31] Grev, R. S., Schaefer III, H. F., and Gaspar, P. P., 1991, *J. Am. Chem. Soc.*, **113,** 5638.
[32] Fukushima, M., Mayama, S., and Obi, K., 1992, *J. Chem. Phys.*, **96,** 44.
[33] Grev, R. S., and Schaefer III, H. F., 1992, *J. Chem. Phys.*, **97,** 8389.
[34] Ishikawa, H., and Kajimoto, O., 1993, *J. Molec. Spectrosc.*, **160,** 1.
[35] Duxbury, G., Alijah, A., and Trieling, R. R., 1993, *J. Chem. Phys.*, **98,** 811.
[36] Gabriel, W., Rosmus, P., Yamashita, K., Morokuma, K., and Palmieri, P., 1993, *Chem. Phys.*, **174,** 45.
[37] Fukushima, M., and Obi, K., 1994, *J. Chem. Phys.*, **100,** 6221 and references cited therein.
[38] Cramer, C. J., Dulles, F. J., Storer, J. W., and Worthington, S. E., 1994, *Chem. Phys. Lett.*, **218,** 387.
[39] Ishikawa, H., and Kajimoto, O., 1995, *J. Molec. Spectrosc.*, **174,** 270.
[40] Matsunaga, N., Koseki, S., and Gordon, M. S., 1996, *J. Chem. Phys.*, **104,** 7988.
[41] Yamaguchi, Y., van Huis, T. J., Sherrill, C. D., and Schaefer III, H. F., 1997, *Theor. Chem. Acc.*, **97,** 341.
[42] Havlas, Z., Downing, J. W., and Michl, J., 1998, *J. Phys. Chem.* A, **102,** 5681.
[43] Escribano, R., and Campargue, A., 1998, *J. Chem. Phys.*, **108,** 6249.
[44] Hiroota, E., and Ishikawa, H., 1999, *J. Chem. Phys.*, **110,** 4254.
[45] Slipchenko, L. V., and Krylov, A. I., 2002, *J. Chem. Phys.*, **117,** 4694.
[46] Nakajima, M., Kawai, A., Fukushima, M., and Obi, K., 2002, *Chem. Phys. Lett.*, **364,** 99.
[47] Ishikawa, H., Muramoto, Y., and Mikami, N., 2002, *J. Molec. Spectrosc.*, **216,** 90.
[48] Kalemos, A., Mavridis, A., and Metropoulos, A., 1999, *J. Chem. Phys.*, **111,** 9536.
[49] Kalemos, A., Mavridis, A., and Metropoulos, A., 2002, *J. Chem. Phys.*, **116,** 6529.
[50] Jacox, M. E., 2003, *J. Phys. Chem. Ref. Data*, **32,** 17.
[51] Jacox, M. E., 2003, Vibrational and electronic energy levels of polyatomic transient molecules, *NIST Chemistry Webbook,* NIST Standard Reference Database Number 69, edited by P. J. Linstrom and W. G. Mallard (Gaithersburg MD: National Institute of Standards and Technology), 20899 (http://webbook.nist.gov).
[52] Dunning Jr, T. H., 1989, *J. Chem. Phys.*, **90,** 1007; Wilson, A. K., van Mourik, T., and Dunning Jr, T. H., 1997, *J. Molec. Spectrosc. (Theochem)*, **388,** 339; Woon, D. E., and Dunning Jr, T. H., 1993, *J. Chem. Phys.*, **98,** 1358; Peterson, K. A., and Dunning Jr, T. H., 2002, *J. Chem. Phys.*, **117,** 10548.
[53] Peterson, K. A., Woon, D. E., and Dunning Jr, T. H., 1994, *J. Chem. Phys.*, **100,** 7410. Basis sets were obtained from the Extensible Computational Chemistry Environment Basis Set Database, Version 12/03/03, as developed and distributed by the Molecular Science Computing Facility, Environmental and Molecular Sciences Laboratory which is part of the Pacific Northwest Laboratory, PO Box 999, Richland, Washington 99352, USA, and funded by the US Department of Energy. The Pacific Northwest Laboratory is a multi-program laboratory operated by Battelle Memorial Institute for the US Department of Energy under contract DE-AC06-76RLO 1830. Contact David Feller or Karen Schuchardt for further information.
[54] MOLPRO, a package of *ab initio* programs designed by H.-J. Werner and P. J. Knowles, version 2002.6, with contributions from R. D. Amos, A. Bernhardsson, A. Berning, P. Celani, D. L. Cooper, M. J. O. Deegan, A. J. Dobbyn, F. Eckert, C. Hampel, G. Hetzer, P. J. Knowles, T. Korona, R. Lindh, A. W. Lloyd, S. J. McNicholas, F. R. Manby, W. Meyer, M. E. Mura, A. Nicklass, P. Palmieri, R. Pitzer, G. Rauhut, M. Schütz, U. Schumann, H. Stoll, A. J. Stone, R. Tarroni, T. Thorsteinsson and H.-J. Werner.
[55] Martin, W. C., and Zalubas, R., 1983, *J. Phys. Chem. Ref. Data*, **12,** 323.
[56] Sam, R. S., Engleman Jr, R., and Bernath, P. F., 1998, *J. Molec. Spectrosc.*, **190,** 341.
[57] Larsson, M., 1987, *J. Chem. Phys.*, **86,** 5018.
[58] Stephens, J. C., Yamaguchi, Y., Sherrill, C. D., and Schaefer III, H. F., 1998, *J. Phys. Chem.* A, **102,** 3999.
[59] van Huis, T. J., Yamaguchi, Y., Sherrill, C. D., and Schaefer III, H. F., 1997, *J. Phys. Chem.* A, **101,** 6955.
[60] Huber, K. P., and Herzberg, G., 2003, Constants of diatomic molecules (data prepared by J. W. Gallagher and R. D. Johnson, III), NIST Chemistry Webbook, NIST Standard Reference Database Number 69, edited by P. J. Linstrom and W. G. Mallard (Gaithersburg MD: National Institute of Standards and Technology), 20899 (http://webbook.nist.gov).
[61] Bruna, P. J., Hirsch, G., Peyerimhoff, S. D., and Buenker, R. J., 1981, *Molec. Phys.*, **42,** 875.